Supporting Information

A 3D real-scale, biomimetic and biohybrid model of the blood-brain barrier fabricated through two-photon lithography

Attilio Marino, Omar Tricinci*, Matteo Battaglini, Carlo Filippeschi, Virgilio Mattoli, Edoardo Sinibaldi,* Gianni Ciofani**

Dr. A. Marino, M. Battaglini, Prof. G. Ciofani
Istituto Italiano di Tecnologia, Smart Bio-Interfaces, Viale Rinaldo Piaggio 34, 56025, Pontedera, Italy

Dr. O.Tricinci, C. Filippeschi, Dr. V. Mattoli, Dr. E. Sinibaldi,
Istituto Italiano di Tecnologia, Center for Micro-BioRobotics, Viale Rinaldo Piaggio 34, 56025 Pontedera, Italy

M. Battaglini
Scuola Superiore Sant'Anna, The BioRobotics Institute, Viale Rinaldo Piaggio 34, 56025 Pontedera, Italy

Prof. G. Ciofani
Politecnico di Torino, Department of Mechanical and Aerospace Engineering, Corso Duca degli Abruzzi 24, 10129 Torino, Italy

E-mails: attilio.marino@iit.it, omar.tricinci@iit.it, edoardo.sinibaldi@iit, gianni.ciofani@iit.it

Experimental Section

Model-based design of the 3D microfluidic chip

In order to substantiate the assumption of $n_t = 50$ flows occurring in parallel, we preliminarily verified to have n_t identical tube inlet conditions in spite of the actual inlet / junction structures. To the purpose, we considered a 2D geometry, for simplicity. In particular, we considered n_t (rectangular) non-porous channels having 10 μm width, for consistency, and we introduced (rectangular) struts as needed for the structural support of the junctions. The considered geometry, sketched in **Figure 2a** (half domain, by symmetry), was exploited for solving the classical Navier-Stokes equations for an incompressible fluid[1] (in the low-Reynolds-number regime) through a commercial finite element solver (Comsol Multiphysics) available to the group.

To the purpose, we adopted a working fluid having 10^3 kg m^{-3} density and 10^{-3} Pa s dynamic viscosity (serum-free cell culture medium). Moreover, we set the inlet flow rate so as to obtain nearly 1 μl h^{-1} in each channel when assuming10 μm height (consistently with the starting assumption on the flow speed magnitude), and we preliminary set-up the numerical solver so as to obtain discretization-independent results. The fluid speed is shown in **Figure 2a** and **2b** (intensity plots); the latter subfigure, in particular, shows that the struts locally affected the flow filed, yet in correspondence to the microcapillaries inlet section (denoted by abscissa x_{T1}) the flow was uniform. This is further remarked by **Figure 2c** that shows the axial velocity profiles obtained through cut-sections immediately before and after (distance $\delta = 0.01$ μm) the considered inlet section. Let us remark that in the present context the absolute magnitude of the velocity profiles in **Figure 2c** was not of interest: the fact that they were uniform was the sought result, which let us proceed by addressing in more detail the flow in a single tube.

As remarked in the main text, the considered continuous problem (**Equation 4**) approximates the

real one, for which spillage only occurs at discrete pores. Hence, we assessed the accuracy of our approach by solving the 3D fluidic problem by means of the previously mentioned numerical solver. In more detail, to contain computational costs we leveraged symmetry: we only considered the domain fraction sketched in **Figure 2f** by imposing periodic boundary conditions on the relevant sagittal cut planes. We adopted the previously mentioned geometric and physical parameters, and we preliminary set-up the numerical ingredients so as to obtain discretization-independent results. Illustrative numerical results of the numerical simulations are shown in **Figure 2g** and **2h**, together with the corresponding analytical solutions. **Figure 2g**, in particular, corresponds to the case at given outlet pressure (associated with **Equation 5**). We chose L =400 μm for the residual flow rate fraction at the outlet, namely $2/(\exp(\hat{L}) + \exp(-\hat{L}))$ based on **Equation 5**, to be practically negligible (order of 10^{-3}). **Figure 2h** corresponds to the case at given outlet flow rate (associated with **Equation 6**), and we adopted ω = 0.4 for the sake of illustration. Based on the considered results, the analytical solution suitably predicted the relevant pressure and flow rate trends, for both outlet conditions. We also experimentally verified the predicted flow behavior; for instance, we fully confirmed that no detectable flow reached the external discharge domain when performing negative control experiments.

Two-photon lithography of the 3D microfluidic chip

The geometry of the microfluidic chip (**Figure S1a**) was modeled with Blender (www.blender.org). The structure is composed of an array of microcapillaries with surface holes in the median region, two junctions, and two connectors for the external tubes. In the bioinspired blood-brain barrier region there are 50 capillaries with internal diameter of 10 μm and length of 800 μm. The middle region, 400 μm in length, is characterized by the presence of 1 μm diameter pores, radially distributed along the cylindrical surface of the capillaries (**Figure S1b-d**). Capillaries were fabricated on a grid for ensuring proper adhesion on the substrate (**Figure**

S1e).

The microfluidic chip was fabricated in negative tone IP-DiLL photoresist (Nanoscribe GmbH) on a glass substrate, by means of a direct laser lithography setup, Photonic Professional system (Nanoscribe GmbH), based on two-photon polymerization. The substrate was rinsed with acetone, isopropyl alcohol (IPA) and deionized water. A drop of IP-DiLL photoresist was cast on the substrate and then the objective (63x, NA 1.4) of the instrument was put in immersion in the photoresist. The microfluidic chip was fabricated by exposing the photoresist to a laser beam (Calman laser source) with a center wavelength of 780 nm, using different writing parameters according to the different geometries of the elements. A writing speed of 10 mm s^{-1} with a laser power of 70.2 mW was used for the capillaries, a writing speed of 10 mm s^{-1} with a laser power of 57.6 mW for the junctions, and a writing speed of 25 mm s^{-1} with a laser power of 108 mW for the connectors. The sample was then developed for 30 min in SU-8 Developer (MicroChem Corp) and rinsed with IPA and deionized water, in order to ensure the proper removal of the uncured photoresist inside the capillaries. The microfabrication results are illustrated in **Figure S2**.

In order to connect the microfluidic chip with the external pumping system, two pipes (20 cm and 1 cm long, respectively) with 50 μm and 280 μm of internal and external diameters, respectively, were linked to the connectors, whose internal cavity has a diameter of 300 μm. This procedure was performed using a micromanipulator under an optical microscope. The connections were sealed by means of a photocurable acrylic glue (Loctite 4305 Flashcure, Henkel AG& Co KGaA), exposed to UV light for 5 minutes (**Figure S3**). Finally, the glass with the microfluidic chip was fixed in a petri dish for the following experiments.

For the scanning electron microscopy (SEM) imaging, microfluidic systems were let dry for at least 2 h and gold-sputtered (10 nm thick layer). The observation was carried out with a Helios

NanoLab 600i FIB / SEM system (FEI).

Cell culture and staining

Immortalized cerebral cortex-derived endothelioma bEnd.3 cell line (ATCC® CRL-2299™) was adopted as a model of brain endothelial cells. bEnd.3 cell monolayer represents a convenient and useful BBB model, especially for testing the paracellular route of transport, owing to the low permeability to sodium fluorescein and to the high expression of tight junctions (even higher with respect to other *in vitro* endothelial models, such as bEnd.5 cells, mouse brain endothelial cell, and primary mouse brain endothelial cells).[2] The transendothelial electrical resistance (TEER) of bEnd.3-based BBB models is comparable to that one of other endothelial models, such as human brain microcapillaries endothelial cells (100 Ω cm^2) and human umbilical vein endothelial cells (74 Ω cm^2 at passage 3).[3]

bEnd.3 cells were cultured in T75 flasks with Dulbecco's Modified Eagle's Medium (DMEM), supplemented with 10% fetal bovine serum (FBS), 2 mM L-glutamine, 100 U ml^{-1} penicillin and 100 μg ml^{-1} streptomycin. They were split every 2-3 days with a subcultivation ratio of 1:10, and, before the experiments, seeded at 100% of confluence (1.3 10^5 cells cm^{-2}) on the 3D capillaries. After 3 days of culture, immunofluorescence staining was performed. Specifically, samples were rinsed with PBS and subsequently fixed with 4 % paraformaldehyde (PFA) in PBS for 20 min at 4°C. The immunostaining against *zonula occludens-1* (ZO-1), also known as tight junction protein-1, allowed the identification of tight junctions,[4] and was carried out by following standard immunocytochemistry procedures. Briefly, samples were incubated with a diluted solution (10 % goat serum in PBS) of a rabbit IgG primary antibody against ZO-1 (Invitrogen, 1:100, 3 h at room temperature) in PBS supplemented with 10 % of goat serum rabbit. Subsequently, samples were repetitively washed (5 washes with 10 % goat serum in PBS) and incubated with a solution of goat Alexa Fluor 488-IgG antirabbit secondary antibody

(Invitrogen). TRITC-conjugated phalloidin (Sigma) and Hoechst (Millipore) were also added to this solution to stain cell cytoskeleton and nuclei, respectively, by following manufacturers' protocols.

With the future perspective of testing anticancer agents, human glioblastoma cancer cells (U-87 MG, ATCC® HTB-14™) were co-cultured with bEnd.3 in the biohybrid system. Before starting the co-cultures, in order to identify the different cell types, bEnd.3 and U-87 cells were stained with fluorescent lipophilic tracers, dialkylcarbocyanine DiD (Invitrogen; excitation and emission peaks at 644 nm and 655 nm, respectively), and dialkylcarbocyanine DiI (Invitrogen; excitation and emission peaks at 549 nm and 565 nm, respectively).

Biological samples dedicated to SEM imaging were fixed with 4 % PFA in PBS for 20 min at 4°C and then rinsed with deionized H_2O. Subsequently, they were incubated with a 2.5 % glutaraldehyde aqueous solution at 4 °C for 30 min. Dehydration steps were carried out by subsequent incubations with increasing ethanol solutions (from 0 % to 100 % in deionized H_2O); samples were finally dried, gold-sputtered, and observed with the SEM. Pore area was thresholded, selected and measured through ImageJ (http://rsbweb.nih.gov/ij/) and the equivalent radius pore was plotted in the density plot with *R* software (https://www.r-project.org/).

Confocal laser scanning microscopy (CLSM, C2S Nikon) was carried out on both living co-cultures (stained with DiD and DiI) and fixed cells (stained for ZO-1, f-actin, and nuclei). The 3D reconstruction of the different *z*-stacks was carried out with the NIS element software.

Trans-endothelial electrical resistance and permeability measurements

Trans-endothelial electrical resistance (TEER) and permeability of the BBB model were both measured before and after seeding the bEnd.3 cells on the porous capillaries. Before both the experiments, two drops of 100 µl phenol red-free DMEM were deposited on the outflow and in the extratubular regions.

TEER was estimated by using a commercially available system (Millipore, Millicell® ERS-2 Voltohmmeter) with an electrode positioned in the outflow liquid and an electrode positioned in the extratubular fluid, close to the porous region.

Fluorescent dextrans represent a valuable and well-characterized tool to study and to compare the permeability both *in vivo* and on *in vitro* models of the BBB.[5,6] Permeability was estimated by pumping the inflow solution (phenol red-free DMEM) modified with 40 μg ml^{-1} of Alexa Fluor 647-conjugated dextran (molecular weight 10000 g mol^{-1}; Thermofisher) in the microfluidic system with a flow rate of 50 μl h^{-1}. The fluorescence time lapse acquisition was performed on the porous region of the microvessels and on the surrounding area of the extratubular fluid with a 10 X magnification objective mounted on an Eclipse Ti-E epifluorescence microscope. The average fluorescence intensity (*F*) was measured at all the time points in two regions of interests (ROI1 and ROI2; **Figure 3e**) and was finally converted to dextran concentration values by using the calibration curve reported in **Figure S6a**. This measure allowed us to monitor on real time the local concentration of the fluorescent dye.

In order to estimate the final concentration of the fluorescent dye in the extratubular region, after 4 minutes of experiment, 50 μl of both the outflow and the extratubular medium were collected and the fluorescence intensity was measured through a spectrofluorimeter (Cary Eclipse fluorescence spectrophotometer, Agilent Technologies). The fluorescence values were subsequently converted in concentrations of dextran through the calibration curve reported in **Figure S6b**.

Supporting References

[1] L. D. Landau, E. M. Lifshitz, Fluid Mechanics: Volume 6 (Course of Theoretical Physics), Butterworth-Heinemann, Amsterdam u.A, **1987**.

[2] T. Watanabe, S. Dohgu, F. Takata, T. Nishioku, A. Nakashima, K. Futagami, A. Yamauchi, Y. Kataoka, *Biol. Pharm. Bull*. **2013**, *36*, 492.

[3] S. Man, E. E. Ubogu, K. A. Williams, B. Tucky, M. K. Callahan, R. M. Ransohoff, *Clin. Dev. Immunol.* **2008**, *2008*, 384982.

[4] J. M. Anderson, A. S. Fanning, L. Lapierre, C. M. Van Itallie, *Biochem. Soc. Trans.* **1995**, *23*, 470.

[5] A. Hoffmann, J. Bredno, M. Wendland, N. Derugin, P. Ohara, M. Wintermark, *Transl. Stroke Res.* **2011**, *2*, 106.

[6] G. Li, M. J. Simon, L. M. Cancel, Z.-D. Shi, X. Ji, J. M. Tarbell, B. Morrison, B. M. Fu, *Ann. Biomed. Eng.* **2010**, *38*, 2499.

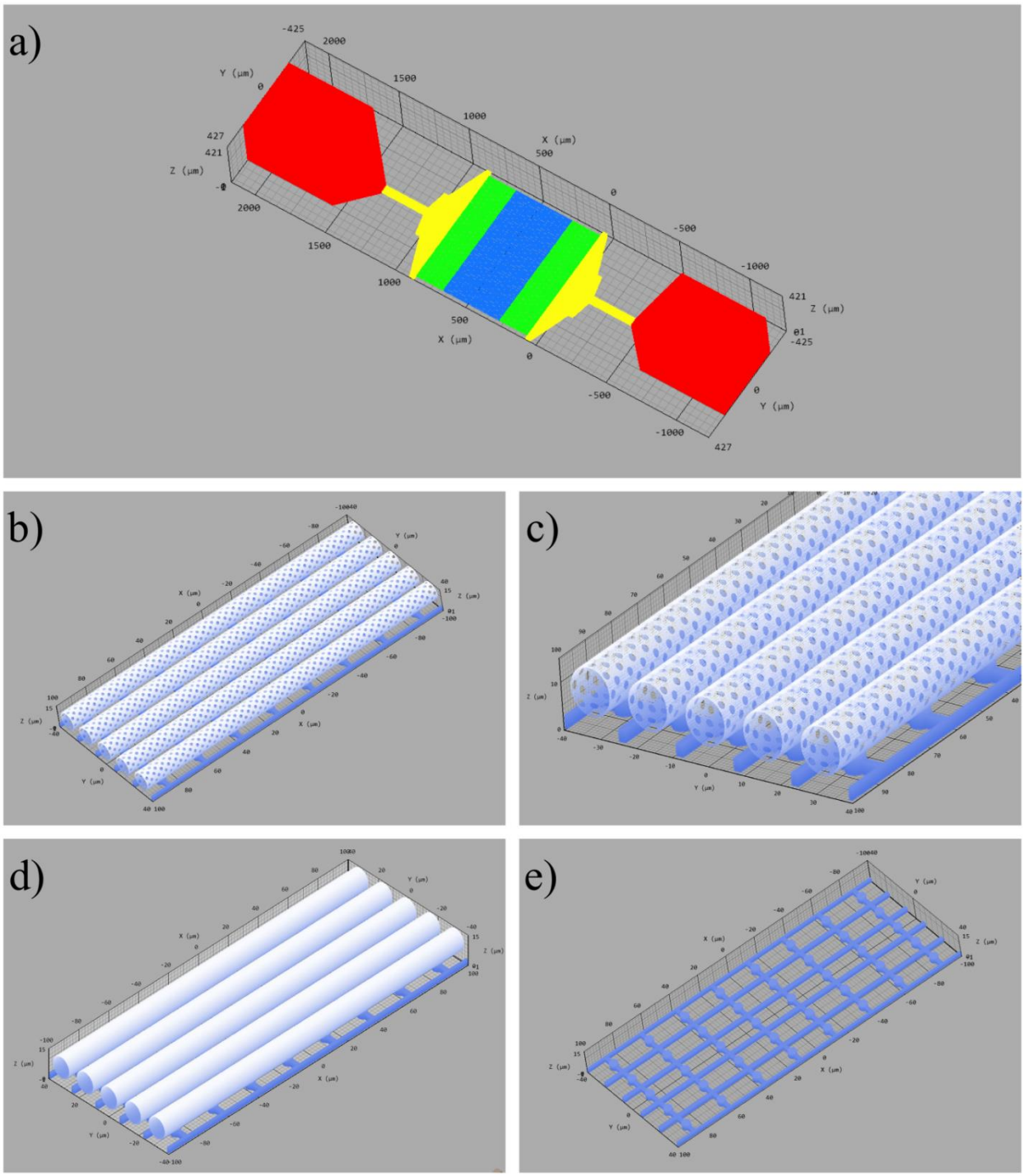

Figure S1. a) Design of the microfluidic chip rendered with DeScribe (Nanoscribe GmbH), with the components labeled in different colors: the connectors in red, the junctions in yellow, capillaries with (in blue) and without (in green) holes. b, c) Details of a portion of the capillaries with holes. d) Detail of the capillaries without holes. e) Base of the capillaries for the anchoring of the structure onto the glass substrate.

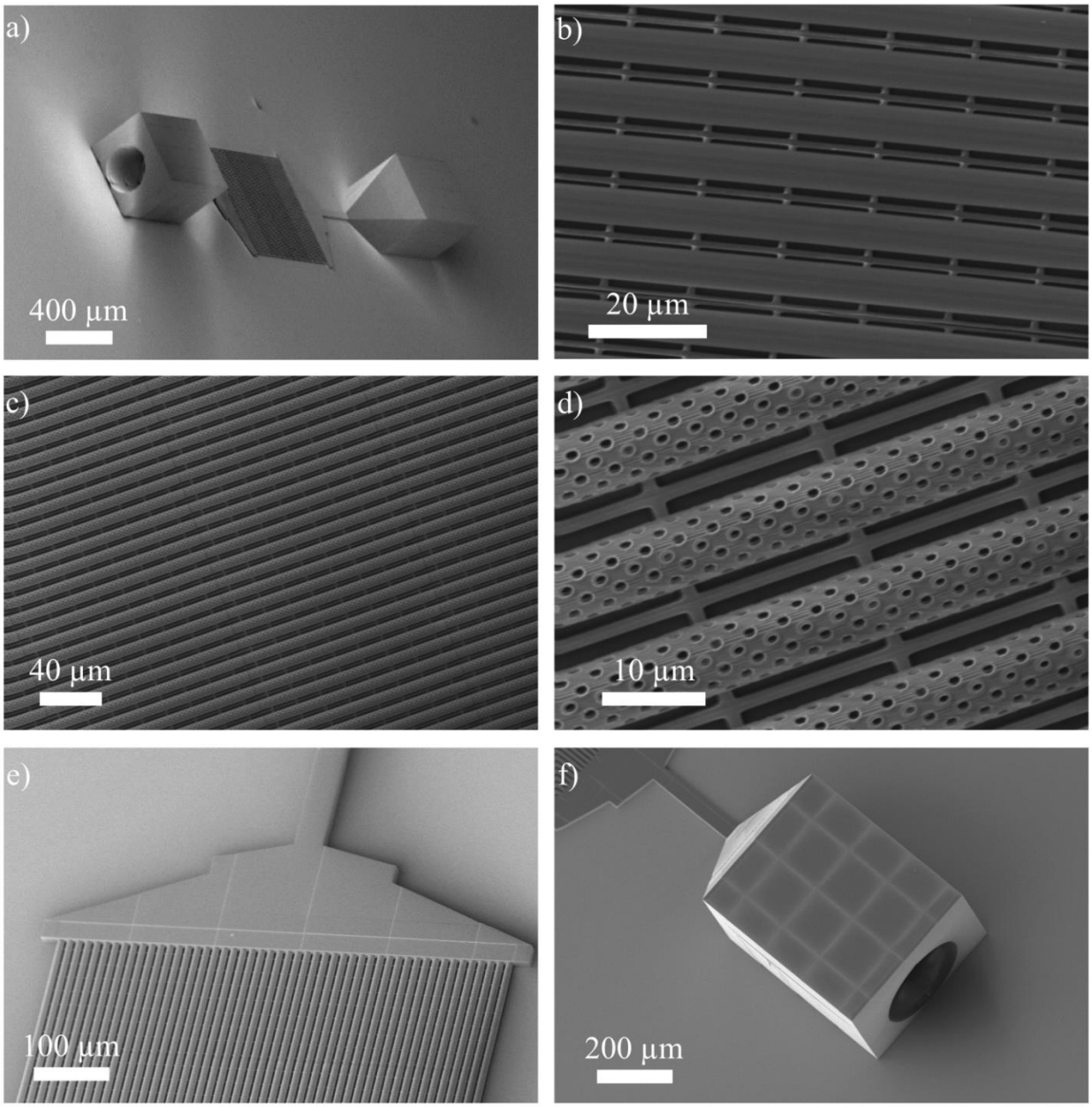

Figure S2. Results of the microfabrication with direct laser lithography; all the images have been acquired with a scanning electron microscope. a) Image of the microfluidic chip. b) Detail of the capillaries without holes. c, d) Detail of the capillaries with holes at different magnifications. e) One of the junctions for the capillaries. f) One of the connectors to the external tubes.

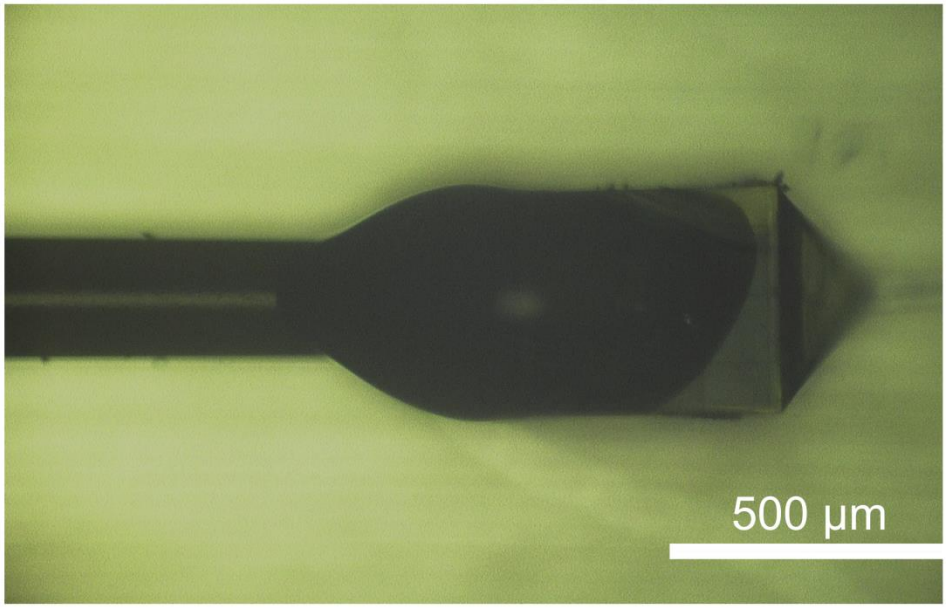

Figure S3. Optical image of the external peek tubes sealed at the connectors of the microfluidic chip.

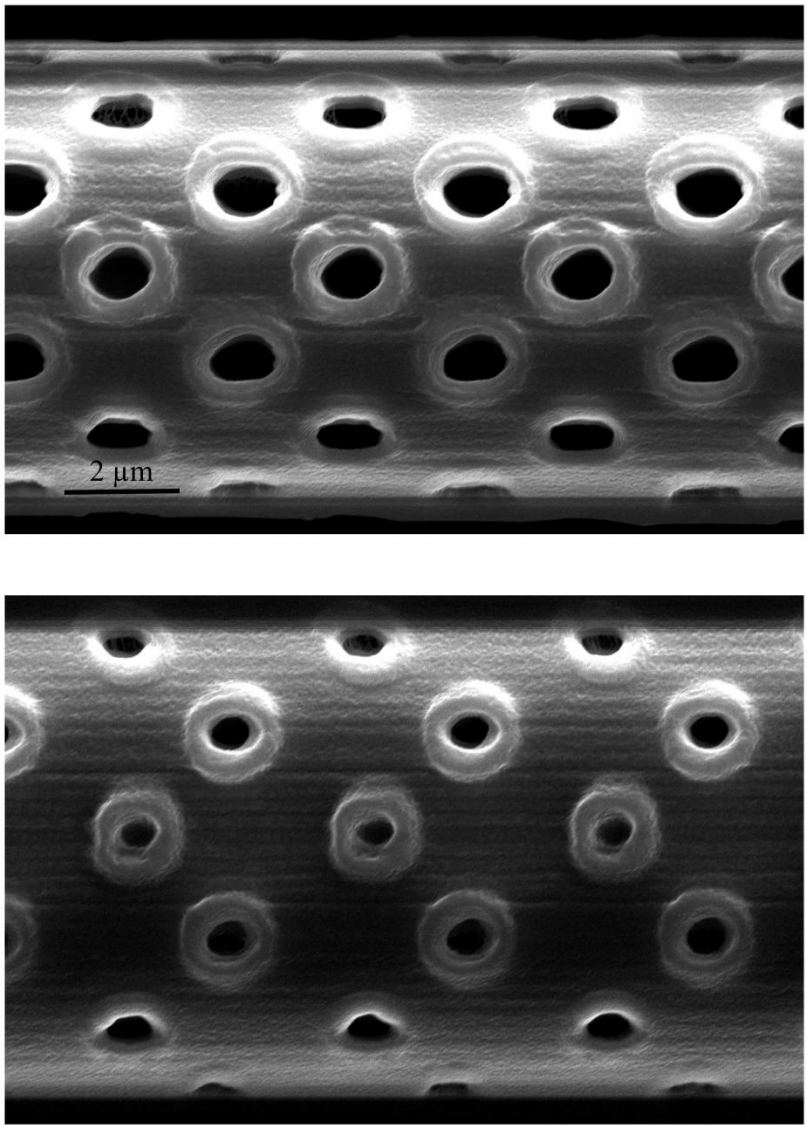

Figure S4. High magnification SEM images of the microcapillaries fabricated with different pore size (about 1.0 µm and 0.5 µm, upper and lower respectively).

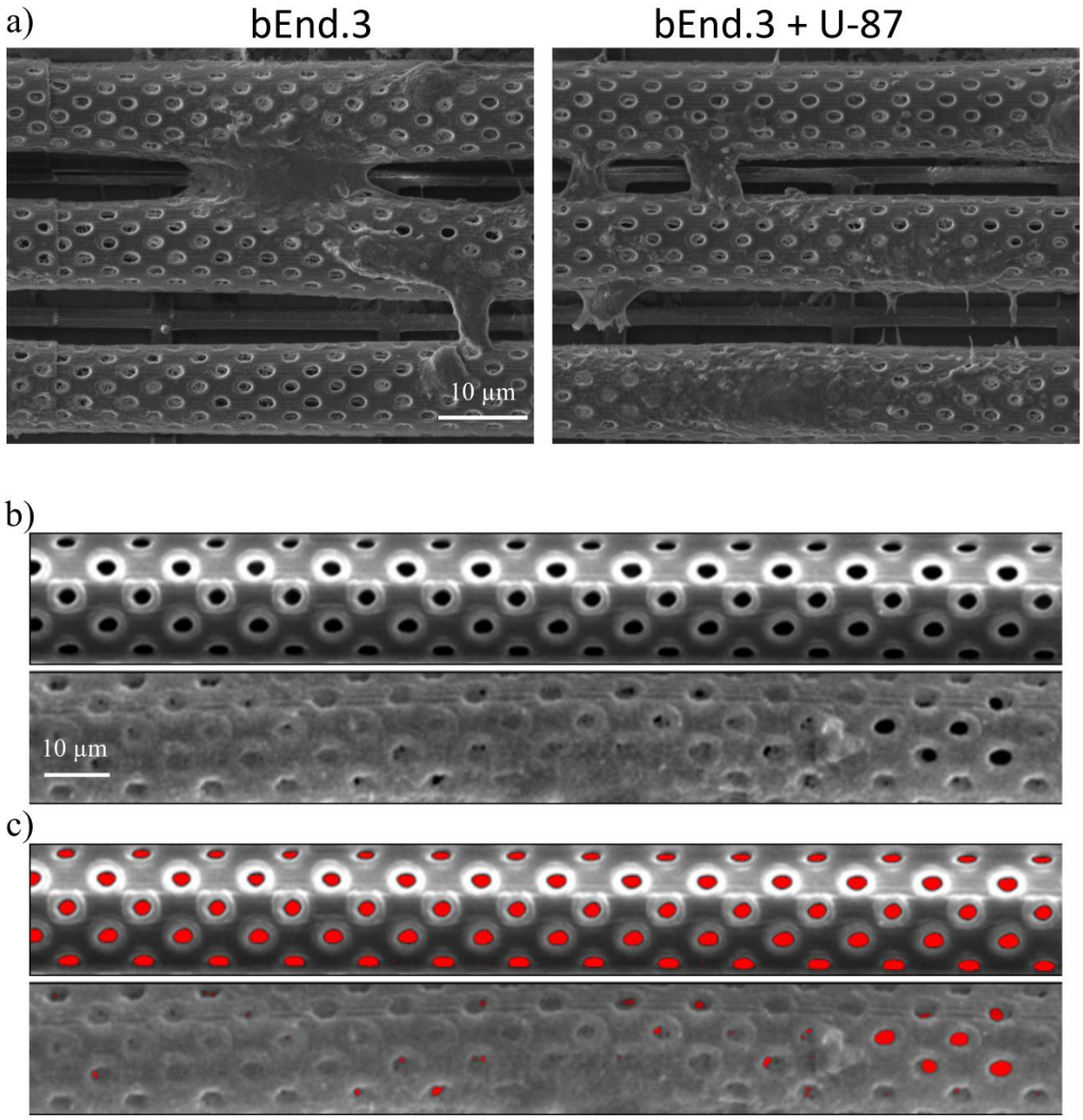

Figure S5. a) Low-magnification SEM images of microcapillaries with bEnd.3 cell culture (image on the left) or bEnd.3 / U-87 co-culture (image on the right). b) Details of microcapillaries before and after bEnd.3 culture (upper and lower image, respectively); c) Selection by threshold of the porous area (in red) related to the images in b).

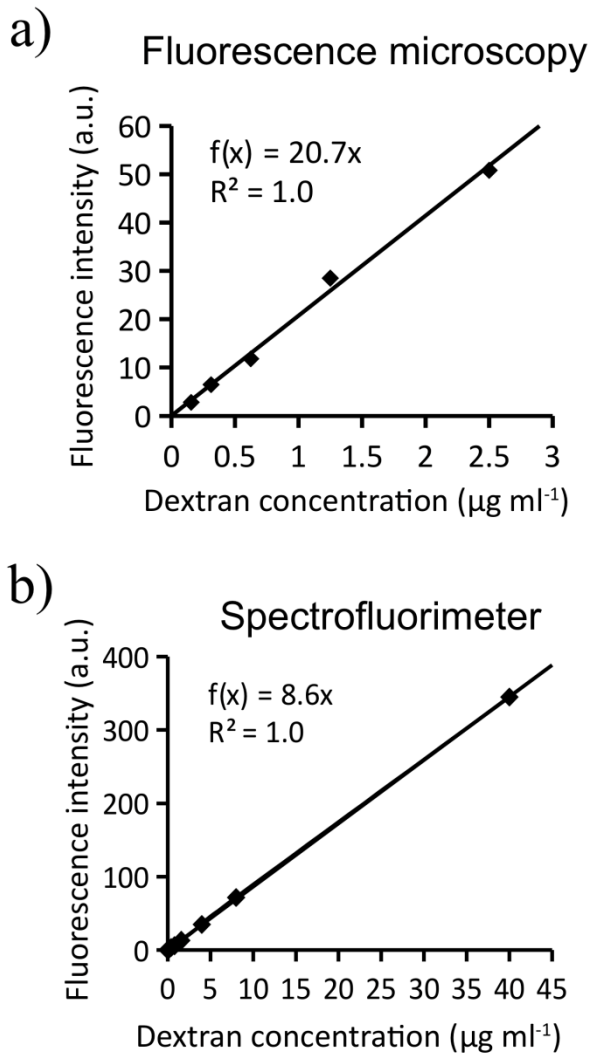

Figure S6. Calibration curves for the assessment of the fluorescent concentration through a) fluorescence microscopy and b) spectrofluorimeter.

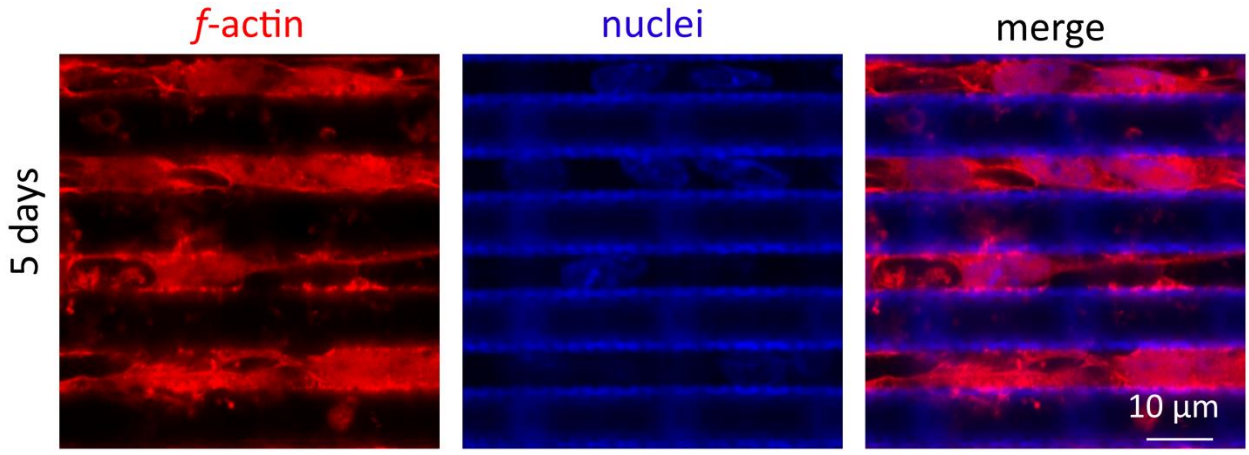

Figure S7. Confocal laser scanning microscopy of bEnd.3 cells cultured for 5 days on 3D porous microcapillaries (*f*-actin in red; nuclei in blue).

Video S1. 3D rendering of confocal *z*-stacks of bEnd.3 cells (nuclei in blue) located all around the microcapillaries.